AIAA JOURNAL
Vol. 30, No. 7, July 1992

Aerodynamic Characteristics of Hoar Frost Roughness

R. J. Kind* and M. A. Lawrysyn†
Carleton University, Ottawa, Canada K1S 5B6

Boundary-layer measurements were carried out in the flow over six preserved samples of frost grown on aluminum plates exposed to the clear night sky. The objective of the work was to determine effective height and spacing characteristics of the frost. This was achieved by examining the effects of the frost roughness on the logarithmic portion of the velocity profiles near the frosted surfaces. It was shown that suitable height and spacing parameters could be determined from the geometry of the higher formations of the frost samples. The ratio of equivalent sand roughness height to average frost formation height varies widely between frost samples.

Nomenclature

A, B	= constants in logarithmic law of the wall
A_F, A_w	= average frontal and windward wetted area, respectively, of roughness elements
C	= function of roughness spacing; see Eq. (2)
C_f	= skin friction coefficient, $\tau_w/0.5\rho U^2$
D	= D^2 is the average surface area occupied by each roughness element or frost formation
H	= boundary-layer shape factor, δ^*/θ
k, k_f, k_s	= effective roughness height, height of highest 20% of frost formations and equivalent sand roughness height, respectively
u, U	= velocity in boundary layer and of freestream, respectively
u^*	= friction velocity, $\sqrt{\tau_w/\rho}$
$\Delta u/u^*$	= see Eq. (1)
x	= distance from leading edge of frost plate
y	= distance above frost plate
δ, δ^*	= boundary-layer thickness and displacement thickness, respectively
θ	= boundary-layer momentum thickness
λ	= roughness-element spacing parameter
λ_D, λ_s	= Dirling and Simpson roughness-element spacing parameters; see Eqs. (5) and (6)
ν	= kinematic viscosity
ρ	= fluid density
τ_w	= wall shear stress
ϕ, ϕ_1, ϕ_2, ϕ_3	= frost formation area factors; see Eq. (7)

Introduction

IT is known that hoar frost on the lifting surfaces of aircraft can have serious negative effects on maximum lift coefficient and drag coefficient, and, thus, also on take-off performance.[1] A layer of 0.5-mm-thick frost on an airfoil of 5-m chord could result in a doubling of drag coefficient and a 30% reduction of maximum lift coefficient.[2,3] A number of studies on the effects of frost have been conducted.[2-6] Frost effects were represented typically by assumed roughness characteristics in analytical studies and by sand roughness in experimental studies. The roughness characteristics or sand roughness heights were based on judgement because there were no established equivalences between frost roughness and sand or other types of roughness.

In the present investigation, measurements were made of boundary layers developing along flat plates covered with actual (preserved) frost. The objective of the work was to determine the aerodynamic characteristics of actual, naturally grown frost-roughness samples.

Six different frost samples were tested. The samples were grown naturally by exposing aluminum plates to the night sky. The frost samples were preserved using a dissolved plastic solution. The plates, covered with preserved frost, were later placed on the test section floor of a low-speed wind tunnel for the boundary-layer measurements. From these measurements, conclusions were drawn regarding effective roughness height and spacing of the frost roughness.

With this information, calculations of the aerodynamic performance of frost-covered lifting surfaces can be carried out with reasonable assurance that the effects of frost are realistically represented. The calculations could, for example, be carried out using panel-method programs that incorporate viscous interaction effects.[7]

Experiments

As already mentioned, the six frost samples were obtained by exposing plates to the clear night sky during the winter months. The plates were laid outdoors on a 2.5-cm-thick layer of foam thermal insulation and inclined at 15 to 20 deg to the horizontal in order to enhance free-convection mass transfer and, thus, frost growth. The plates were 3 × 759 × 1828 mm, sized to suit the wind-tunnel working section.

The preservation technique was suggested by an article on preservation of snow crystals.[8] A polyvinyl formal plastic material (Monsanto FORMVAR) was dissolved in methylene chloride to form a 0.5% solution by weight. The solution was kept outside so that its temperature was well below the freezing point of water. It was poured gently onto the edge of the frosted plate and would seep down the plate with the excess running off. About 1 liter of solution was required to preserve one frosted plate. According to Schaefer,[9] the solution soaks into the porous frost and the solvent evaporates, leaving a thin plastic film structure. The frozen water sublimates or evaporates through the plastic film as ambient temperature increases. After several hours, only a faithful plastic replica of the frost remains. There is no smoothing or rounding of edges. The accuracy of replication can be judged from Fig. 1. Frost of any shape could be faithfully preserved.

Figure 2 presents photographs of the six samples tested. The preserved frost in these samples was sufficiently robust that no detectable deformation or deterioration occurred during the wind-tunnel testing. The general appearance of the

Received Dec. 14, 1990; presented as Paper 91-0686 at the AIAA 29th Aerospace Sciences Meeting, Reno, NV, Jan. 7–10, 1991; revision received Oct. 25, 1991; accepted for publication Nov. 29, 1991.

*Professor, Department of Mechanical and Aerospace Engineering.
†Graduate Student. Now with the Canadian Armed Forces.

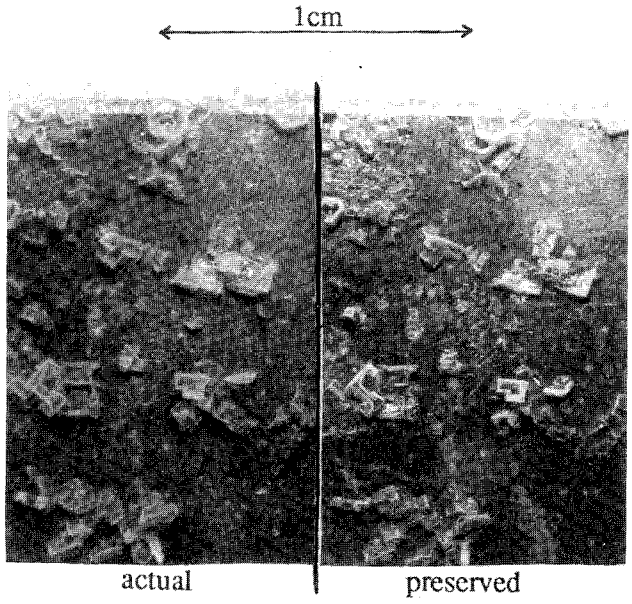

Fig. 1 Actual and preserved frost sample.

frost was basically the same all over each plate, but frost density and height fluctuated considerably over wavelengths of order 0.3 m.

The preserved frost samples were tested in a closed-return wind tunnel having a 0.51 × 0.76 × 1.83-m test section operating at atmospheric pressure. The plates were fastened to the test section floor, which was then entirely covered with preserved frost. The tunnel contraction ratio was 12:1, giving highly uniform flow outside the wall boundary layers; the freestream longitudinal turbulence intensity was about 0.15%. Earlier calibration work[10] had established that two dimensionality in the floor boundary layers was excellent and that lateral variation of skin friction was less than 5% of centerline values. A nominal wind speed of 50 m/s was used for all tests, giving a Reynolds number based on frost-sample length of 5.5×10^6 and greater than 5×10^3, based on boundary-layer momentum thickness. There was a weak favorable pressure gradient along the test section.

Boundary-layer velocity profiles were measured at five stations along the centerline of each frost plate and on the smooth tunnel floor. The boundary layers at station 1 ($x = 0.33$ m) were not yet in equilibrium with the surface roughness and at station 5 ($x = 1.73$ m) some influence of the wind-tunnel diffuser was apparent. Therefore, only data taken at stations 2, 3, and 4 were used. The frost was completely undisturbed upstream of the measurement stations.

Measurements included the following: profiles of pitot pressure at the five measurement stations; static pressure on the tunnel ceiling at five points, each slightly upstream of one of the measurement stations; static pressure drop across the tunnel contraction to determine freestream wind speed. All pressures were sensed by carefully calibrated capacitive differential pressure transducers having a nominal sensitivity of 0.75 V/kPa. Pitot tube positioning accuracy was ±0.02 mm. A displacement correction[11] was applied to the pitot data. Pressures were sampled and processed by a computer data acquisition system. Dynamic pressure was taken as the difference between the pitot reading and the nearest ceiling static-tap reading. The pitot, the static and the tunnel contraction pressures were sampled at each step in the pitot traverses. The current dynamic pressure was then normalized by the current contraction pressure difference so that the velocity ratio data for the boundary layers were not affected by slow drifting of the tunnel operating point. Each pitot traverse comprised about seventy data points over the boundary-layer thickness of about 25 mm. The uncertainty on values of velocity ratio, u/U, is estimated at ±0.001.

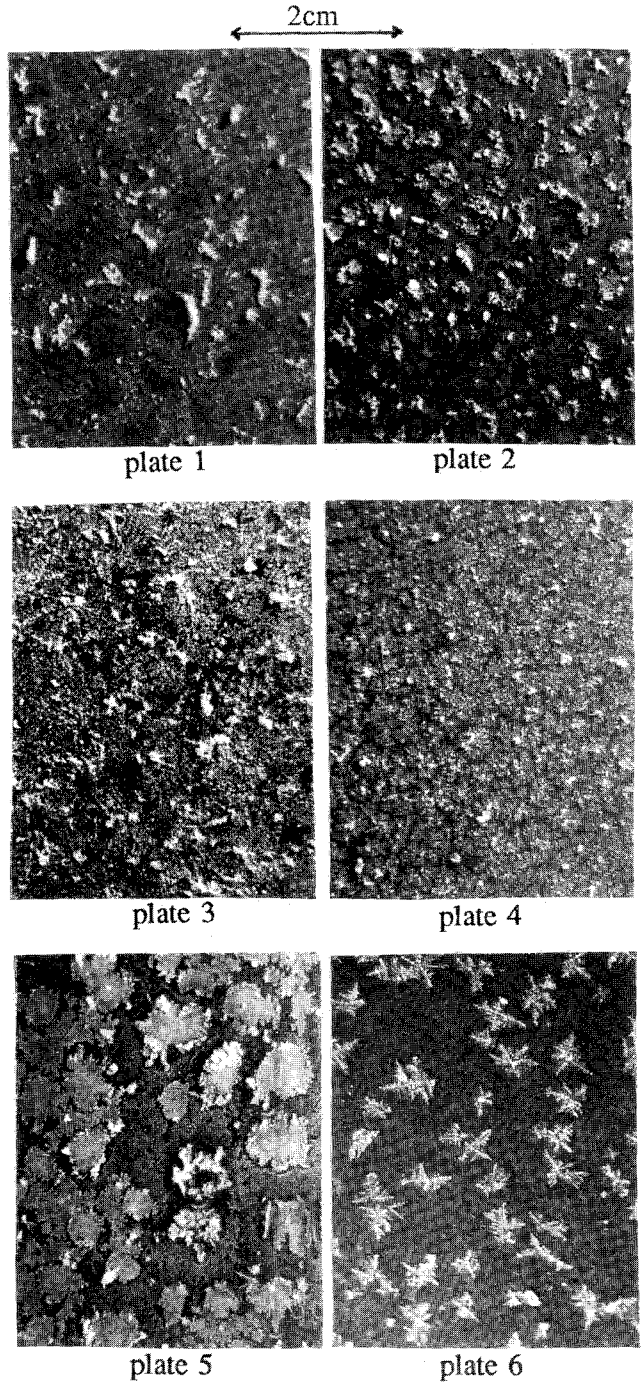

Fig. 2 Partial photographs of the tested frost samples.

Data Analysis and Results

The height of the present frost roughness was much less than the boundary-layer thickness at the measuring stations. That being the case, only the inner portion of the velocity profiles, where, not when the law of the wall prevails, would be affected directly by the roughness.[12] Over rough surfaces in nominally zero pressure gradient, the logarithmic portion of the law of the wall assumes the form[13,14]

$$\frac{u}{u^*} = A\log\left(\frac{yu^*}{\nu}\right) + B - \left(\frac{\Delta u}{u^*}\right) \qquad (1)$$

In the present samples, significant frost formations were quite widely spaced; therefore $y = 0$ at the plate surface. The constants A and B are assigned the values 5.62 and 5.0 respectively. $(\Delta u/u^*)$ is the shift in intercept of the log law. This

shift is due to the surface roughness and for fully rough surfaces it is given by[14]

$$\frac{\Delta u}{u^*} = A\log\left(\frac{ku^*}{\nu}\right) + C[\lambda] \tag{2}$$

C is a constant for any particular type of roughness and its value depends on a spacing parameter, λ, of the roughness. The dependence of C on λ is established from empirical data. The objectives of the present work were to establish a C vs λ correlation for frost roughness and to relate the effective roughness height k to the physical characteristics of the frost.

The velocity profile data are initially available in the form u/U vs y. The skin friction coefficient C_f, is equal to $2(u^*/U)^2$. If C_f can be determined, the velocity profile data can be plotted as u/u^* vs log (yu^*/ν) and $\Delta u/u^*$ can be determined using Eq. (1). Assignment of a value for k then implies a value for C by virtue of Eq. (2). This approach was used to analyze the data.

Because of the $(\Delta u/u^*)$ term in Eq. (1), the conventional Clauser-plotting[12] technique for determining C_f is unsatisfactory for rough-wall boundary layers. C_f values were determined using the two-dimensional momentum integral equation

$$\frac{C_f}{2} = \frac{d\theta}{dx} + (H + 2)\frac{\theta}{U}\frac{dU}{dx} \tag{3}$$

The two derivatives in Eq. (3) were determined from smooth curves drawn through the data. For the smooth plate, the C_f values determined from the momentum equation are in good agreement with those determined by the Clauser-plotting technique (Table 1). This gives confidence in the C_f values and also indicates that two dimensionality of the boundary-layer flows was good.

Clauser[14] has shown that the velocity-defect law applies in the outer region of both smooth and rough wall boundary layers in nominally zero pressure gradient. This provided another technique for estimating C_f values in the present work. The velocity defect law can be written in the form

$$\frac{U - u}{u^*} = A\log\left(\frac{y}{\delta}\right) + D + G_1[y/\delta] \tag{4}$$

The constant D and the function $G_1[y/\delta]$ are established by Clauser's[14] plots of experimental data. Equation (4) can be plotted for various assumed values of $u^*/U = \sqrt{C_f/2}$, in the form u/U vs y/δ. The velocity profile data can be plotted on the same graphs, allowing C_f to be read off. The C_f values determined in this way are included in Table 1. For the smooth plate (no. 7), the C_f values determined by all techniques are in good agreement. Furthermore, the agreement between the momentum equation and the defect law C_fs can also be considered good for the frosted plates, bearing in mind the somewhat random and nonuniform characteristics of the frost roughness. This gives additional confidence in the values of C_f, which is important because the results are quite sensitive to C_f. The uncertainty of C_f values is estimated at ± 0.0004.

Figure 3 illustrates how values of $\Delta u/u^*$ were determined. It is a plot of the data in the format of Eq. (1), with the momentum equation values of C_f used to determine u^*/U for each profile. The shift $(\Delta u/u^*)$ can be read in Fig. 3. Not surprisingly there is considerable scatter in the values of $\Delta u/u^*$ (see Table 1). This reflects the nonuniformity of frost characteristics over each plate as well as the uncertainty of about ± 0.5 on values of $\Delta u/u^*$ at each station. The latter arises mainly from the uncertainty of C_f or u^*/U values. The arithmetic average of the values at stations 2, 3, and 4 is used as the representative value of $\Delta u/u^*$ for each frost plate; these values are shown in Table 2.

Once $\Delta u/u^*$ is determined for each frost sample, the values of k and C are interrelated by virtue of Eq. (2). Thus, the choice of effective roughness height k can be somewhat arbitrary, because for any choice of k, C can still be chosen to satisfy Eq. (2). In previous work with relatively uniform roughness (e.g., spheres, cones, sand, etc.), the overall height of the roughness elements has generally been used for k.[15] For consistency with this past practice, and recognizing the statistical nature of the frost geometry, k was taken to be equal to the average height k_f of the highest 20% of the frost formations of each sample. The use of, say, 10 or 30% instead of 20% would have had little effect. The frost in each of the six samples consisted of relatively high formations scattered over the surface with relatively low background frost covering the intervening space. The average height of the formations could be estimated quite easily by use of a tongue-type feeler gauge and a watchmaker's eyepiece. The stacks of selected

Table 1 Velocity profile characteristics

Frost plate	Stn. no.	x (mm)	U/U_{ref}	θ (mm)	H	C_f mom. eq.	C_f Clauser plot	C_f Defect law	$\Delta u/u^*$
	2	675	1.008	2.57	1.50	0.0054	——	0.0059	7.6
1	3	1025	1.016	3.43	1.45	0.0044	——	0.0050	6.4
	4	1375	1.021	3.98	1.35	0.0039	——	0.0035	4.5
	2	675	1.002	2.18	1.41	0.0038	——	0.0040	3.3
2	3	1025	1.01	2.79	1.38	0.0041	——	0.0037	4.3
	4	1375	1.02	3.38	1.41	0.0043	——	0.0035	5.4
	2	6725	1.008	2.79	1.54	0.0057	——	0.0060	8.3
3	3	1025	1.016	3.66	1.45	0.0053	——	0.0050	6.9
	4	1375	1.024	4.43	1.45	0.0050	——	0.0048	7.6
	2	675	1.007	2.46	1.47	0.0048	——	0.0050	5.0
4	3	1025	1.016	3.20	1.42	0.0050	——	0.0043	6.7
	4	1375	1.024	4.01	1.40	0.0049	——	0.0040	6.7
	2	675	1.006	2.16	1.39	0.0034	——	0.0038	2.3
5	3	1025	1.014	2.74	1.35	0.0036	——	0.0032	2.8
	4	1375	1.015	3.28	1.33	0.0037	——	0.0030	3.2
	2	675	1.007	2.25	1.41	0.0043	——	0.0042	4.6
6	3	1025	1.013	2.78	1.44	0.0040	——	0.0044	4.9
	4	1375	1.020	3.53	1.38	0.0042	——	0.0038	5.2
	1	325	1.000	1.27	1.38	0.0030	0.00325	0.0032	0
7	2	675	1.008	1.80	1.35	0.0030	0.0030	0.0030	0
	3	1025	1.014	2.25	1.33	0.0031	0.00295	0.0029	0
(smooth)	4	1375	1.020	2.25	1.31	0.0032	0.00290	0.0026	0

feeler gauge tongues would be placed next to a frost formation so that the stack and formation heights could be compared. The height of a formation could be estimated within ± 0.05 mm. The height of the highest 20% of frost formations in the present samples was fairly uniform, varying within about $\pm 15\%$. Values of k_f for each frost sample are given in Table 2. Other methods of measuring frost height were tried, including that suggested by Langston,[16] but were found less effective and less convenient. By substituting k_f and other parameters from Table 2 into Eq. (2), a value of C was found for each frost sample. The values are included in Table 2. The values found for C are quite sensitive to the values of u^* or C_f; values of C are subject to an uncertainty of about ± 0.7, due mainly to the uncertainty on values of C_f or u^*/U.

The next requirement was to establish a suitable spacing parameter λ with which C could be correlated. Several authors, including Dvorak,[17] Simpson,[18] and Dirling[19] have proposed roughness spacing parameters. Dvorak's parameter is best suited to two-dimensional (bar) roughness geometries.

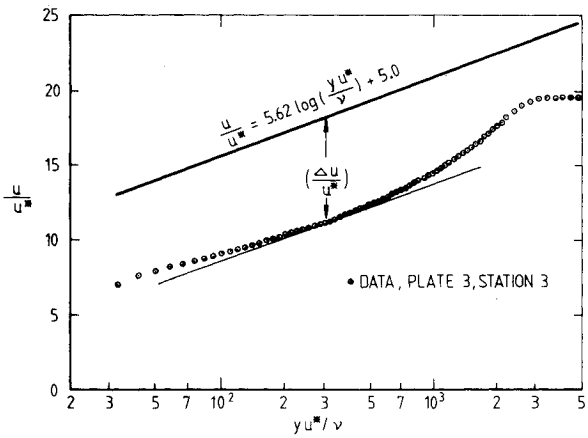

Fig. 3 Technique for determining $\Delta u/u^*$.

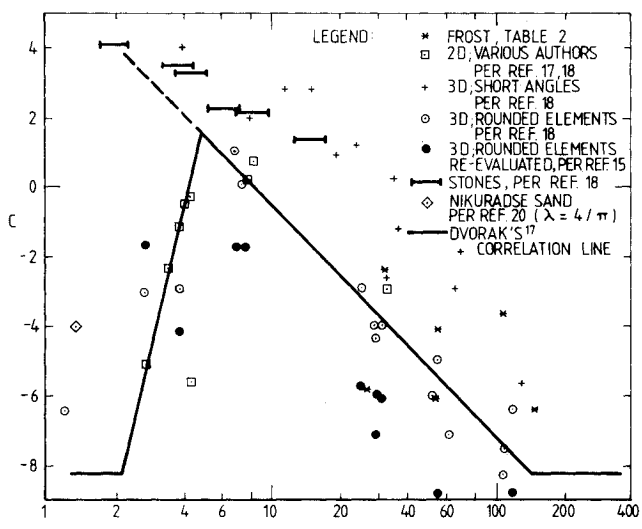

Fig. 4 Correlation between law-of-the-wall intercept shift and roughness spacing parameter (after Dvorak[17] and Simpson[18]).

The Simpson and Dirling parameters, designated λ_s and λ_D, are more suitable to the present application. Simpson defines λ_s as:

$$\lambda_s = D^2/A_F \tag{5}$$

where A_F is the average frontal area of the "significant" roughness elements and $1/D^2$ is equal to the number of significant roughness elements per unit surface area. Dirling defines λ_D as:

$$\lambda_D = (D/k)(A_F/A_W)^{-4/3} \tag{6}$$

where A_W is the wetted area of the windward surface of the roughness elements. D can easily be determined by counting the number of significant frost peaks present over an area of the frost sample. The value of $1/D^2$ for each of the present samples is given in Table 2; the values are subject to an uncertainty of ± 0.5. This arises mainly because deciding which frost formations should be counted (i.e., considered significant) is a matter of judgment. Unfortunately, direct evaluation of A_F and of A_W for frost presents obvious difficulties. The approach adopted herein was to estimate a formation-area factor ϕ for the frost formations such that

$$A_F = \phi k_f^2 \tag{7}$$

The factor ϕ was taken as the product $\phi_1\,\phi_2\,\phi_3$. The frontal projections of the significant frost formations were approximately rectangular for all the frost samples; ϕ_1 represents the average width-to-height ratio of these formations and was estimated visually; and ϕ_2 represents the ratio of the average height of all the significant formations to the height k_f of the highest 20% of the formations, it too was estimated visually. In some of the samples (e.g., plates 3 and 4) there was a substantial amount of "background" frost of relatively low height between the "significant" formations. When background frost covers a large fraction of the surface area, it can be expected to have a significant effect on the flow, although it is of relatively low height. The factor ϕ_3 was used to account crudely for this effect; where background frost was judged to be important, ϕ_3 was assigned a value of 1.5. The values of ϕ_1, ϕ_2, ϕ_3, and ϕ for the six frost samples are listed in Table 2.

Substitution of Eq. (7) into Eq. (5) gives

$$\lambda_s = D^2/\phi k_f^2 \tag{8}$$

Simpson's spacing parameter was preferred to Dirling's because the former could be more readily related to frost formation geometry and because it recognizes frontal area of roughness elements in a manner that seems intuitively more appropriate. The values of λ_s for each frost sample are given in Table 2. Clearly, these are subject to a large uncertainty, estimated at $\pm 50\%$, due to the inherent variability of the frost.

The values of C and λ_s from Table 2 are plotted in Fig. 4 together with data for other types of roughness. Dvorak's[17] correlation line which was also used by Simpson,[18] is included in Fig. 4. The scatter of the frost results in Fig. 4 is very large. However, it is no worse than that of the other data for much more regular roughness configurations. It must be kept in

Table 2 Average parameters of the six frost roughness samples

Frost plate	Mom. Eq. C_f	Mom. Eq. u^*/U	$\Delta u/u^*$	k_f (mm)	$k_f u^*/\nu$	C	$1/D^2$ (cm^{-2})	ϕ_1	ϕ_2	ϕ_3	ϕ	λ_s	k_s/k_f
1	0.0047	0.048	6.2	1.0	140	−5.9	1.8	3	0.7	1	2.1	26	0.46
2	0.0041	0.045	4.3	0.5	70	−6.1	5.0	1.5	1	1	1.5	53	0.43
3	0.0053	0.51	7.6	0.4	62	−2.5	4.5	3	1	1.5	4.5	31	1.8
4	0.0049	0.049	6.1	0.37	56	−3.7	4.5	1	1	1.5	1.5	108	1.1
5	0.0036	0.042	2.8	0.35	47	−6.5	3.0	1	1	1.5	1.5	181	0.36
6	0.0042	0.046	4.9	0.27	40	−4.1	2.5	10	1	1	10	5	0.96

mind that each of the six frost data points in Fig. 4 is for a distinctly different roughness configuration. The large scatter in Fig. 4 mainly reflects shortcomings of the correlation, not of the measurements.

An equivalent sand roughness height k_s can be deduced easily for each of the frost samples. For standard closely spaced sand roughness C has a value of -4.0. This value is based on Grigson's[20] reassessment of Nikuradse's experiments, with A and B of Eqs. (1 and 2) having Coles's[21] recommended values, 5.62 and 5.0, respectively. $\Delta u/u^*$ must be the same for the actual roughness and the equivalent sand roughness. The C and k_f values from Table 2 can, thus, be used with Eq. (2) to calculate the ratio k_s/k_f for each frost sample. The ratios are given in Table 2. They vary widely—this simply reflects the importance of roughness spacing as well as height.

Discussion

Equation (2), which is crucial to the data analysis, only applies if the flow is fully rough, that is, if ku^*/ν exceeds some lower limit. Generally accepted values for the lower limit range from 50 to 70.[22] However, when experimental data for rough-wall boundary layers are plotted in the form $\Delta u/u^*$ vs $\log(ku^*/\nu)$, the plots are linear with slope equal to A for $ku^*/\nu \geq 30$ (see Dvorak's Fig. 1 and also Ref. 20). This implies that Eq. (2) is valid for $ku^*/\nu > 30$. As seen in Table 2, the values of $k_f u^*/\nu$ of the six frost samples satisfy this criterion.

The approach used to arrive at an effective height k_f and spacing-parameter λ_s for the frost roughness is based on the assumption that the higher frost formations (referred to as the significant formations) produce the main aerodynamic effects and that the background frost is only of minor importance. This assumption is supported by Fig. 4, where it is seen that the C vs λ_s results found for the frost samples are consistent with C vs λ_s behavior for roughnesses whose C and λ_s are straightforward to determine.

Boundary-layer development calculated using Dvorak's[17] method, with C values either from the correlation line or from the frost data points in Fig. 4, agrees reasonably well with measured development on the frost plates. This suggests that the effects of the frost roughness are satisfactorily represented by the k_f and λ_s values determined in this investigation.

In recent years, discrete-element calculation methods have appeared. These methods calculate flow development over rough surfaces by considering the roughness elements explicitly and modeling the flow in their vicinity.[23] For these methods, frost roughness could be represented by uniformly distributing elements of height k_f and frontal area ϕk_f^2, with one element per D^2 of the surface area. A value would also have to be assumed for the element drag coefficient.

Conclusions

Boundary-layer development over six preserved samples of natural frost has been measured. The samples were of frost that occurred during clear cold nights. Simple methods have been developed for determining effective height and spacing parameters for the frost roughness samples. An existing correlation, established for roughness elements of simple geometry, can be used to correlate aerodynamic effects with the spacing parameter. The ratio of equivalent sand roughness height to frost height varies widely between frost samples.

Acknowledgment

The authors gratefully acknowledge support from a Natural Sciences and Engineering Research Council operating grant.

References

[1]Luers, J. K., "Wing Contamination: Threat to Safe Flight," *Astronautics and Aeronautics*, Nov. 1983, pp. 54–59.

[2]Ljungström, B. L. G., "Wind Tunnel Investigation of Simulated Hoar Frost on a 2-Dimensional Wing Section With and Without High Lift Devices," Aeronautical Research Institute of Sweden (FFA) Rept. FFA-AU-902, April 1972.

[3]Dietenberger, M. A., "A Simple and Safe Takeoff or Landing Procedure With Wing Surface Contaminations," *Journal of Aircraft*, Vol. 21, No. 12, Dec. 1984, pp. 955–961.

[4]Gregory, N., and O'Reilly, C. L., "Low-Speed Aerodynamic Characteristics of NACA-0012 Aerofoil Section, Including the Effects of Upper-Surface Roughness Simulating Hoar Frost," NPL Aero Report 1308, Ames Research Center (NASA); British Aeronautical Research Council 31719, Jan. 1970.

[5]Weeks, D. J., "Tests on the Effect of Simulated Hoar Frost Deposits on the Take-Off Performance of a Model of a Transport Aircraft (Hawker Siddeley Trident 3B)," Royal Aircraft Establishment TR 71178, Aug. 1971.

[6]Zierten, T. A., and Hill, E. G., "Effects of Wing Simulated Ground Frost on Airplane Performance," von Karman Institute Lecture Series, *Influence of Environmental Factors on Aircraft Performance*," Brussels, Belgium, Feb. 1987.

[7]Maskew, B., and Dvorak, F. A., "Investigation of Separation Models for the Prediction of $C_{L\max}$," American Helicopter Society Paper 77.33-01, May 1977.

[8]Sisson, R. F., "Snowflake Magic," *National Geographic*, Vol. 137, No. 1, Jan. 1970, pp. 104–110.

[9]Schaefer, V. J., "How to Fingerprint a Snowstorm," *Natural History*, Jan. 1943.

[10]Nituch, M. J., "The Use of Congruent Obstacle Blocks for the Indirect Measurement of Turbulent Skin Friction on Smooth Surfaces," Master's Thesis, Carleton University, Ottawa, Canada, 1972.

[11]Ozarapoglu, V., "Measurements in Incompressible Turbulent Flow," Ph.D. Thesis, Univ. Laval, Québec, Québec, Canada, 1973.

[12]Clauser, F. H., "Turbulent Boundary Layers in Adverse Pressure Gradients," *Journal of the Aeronautical Sciences*, Vol. 21, No. 2, 1954, pp. 91–108.

[13]Hama, F. R., "Boundary-Layer Characteristics for Smooth and Rough Surfaces," *Transactions of the American Society of Naval Architects and Marine Engineers*, Vol. 62, No. 563, Nov. 1954, pp. 266–270.

[14]Clauser, F. H., "The Turbulent Boundary Layer," *Advances in Applied Mechanics*, Vol. 4, 1956, pp. 1–51.

[15]Coleman, H. W., Hodge, B. K., and Taylor, R. P., "A Re-Evaluation of Schlichting's Surface Roughness Experiment," *Journal of Fluids Engineering*, Vol. 106, No. 3, 1984, pp. 60–65.

[16]Langston, P. A. S., "Hoar Frost on Aircraft Surfaces," British European Airways Engineering TN P/570, Nov. 1968.

[17]Dvorak, F. A., "Calculation of Turbulent Boundary Layers on Rough Surfaces in Pressure Gradient," *AIAA Journal*, Vol. 7, No. 9, 1969, pp. 1752–1759.

[18]Simpson, R. L., "A Generalized Correlation of Roughness Density Effects on the Turbulent Boundary Layer," *AIAA Journal*, Vol. 11, No. 2, 1973, pp. 242–244.

[19]Dirling, R. B., "A Method for Computing Roughwall Heat Transfer on Re-entry Nosetips," AIAA Paper 73-763, Palm Springs, CA, July 1973.

[20]Grigson, C. W. B., "Nikuradse's Experiment," *AIAA Journal*, Vol. 22, No. 7, 1984, pp. 1000–1001.

[21]Coles, D., "The Young Person's Guide to the Data," Air Force Office of Scientific Research-Internal Flow Program Stanford Conference on the Calculation of Turbulent Boundary Layers, Vol. II, 1968.

[22]Schlichting, H., *Boundary Layer Theory*, 4th ed., McGraw-Hill, New York, 1960.

[23]Taylor, R. P., Coleman, H. W., and Hodge, B. K., "Prediction of Turbulent Rough-Wall Skin Friction Using a Discrete Element Approach," *Journal of Fluids Engineering*, Vol. 107, No. 6, 1985, pp. 251–256.